Examination of the Premelting Transition of DNA A-Tracts Using a Fluorescent Adenosine Analogue†

Katherine E. Augustyn,‡ Kristi Wojtuszewski,‡,§ Mary E. Hawkins,|| Jay R. Knutson,⊥ and Ishita Mukerji*,‡

Molecular Biophysics Program, Molecular Biology and Biochemistry Department, Wesleyan University, Middletown, Connecticut 06459-0175, Pediatric Oncology Branch, National Cancer Institute, National Institutes of Health, Building 10, CRC 1-3872, Bethesda, Maryland 20892, and Laboratory of Biophysical Chemistry, Optical Spectroscopy Section, National Heart, Lung, and Blood Institute, National Institutes of Health, Building 10, Room 5D-14, Bethesda, Maryland 20892-1412

Received September 9, 2005; Revised Manuscript Received January 12, 2006

ABSTRACT: The fluorescent adenosine analogue 4-amino-8-(2-deoxy-β-D-ribofuranosyl)-5′-*O*-dimethoxytrityl-6-methyl-7(8*H*)-pteridone (6MAP) has been used to perform residue specific analyses of DNA A-tracts during the premelting transition. DNA A-tracts, which exhibit sequence-induced curvature, adopt a B-DNA conformation as a function of increasing temperature. Fluorescence melting curves indicate that 6MAP is a more sensitive reporter of the premelting transition than UV absorption spectroscopy. Further, residue specific fluorescence analyses of A-tract and control duplexes reveal that some of the conformational changes associated with the premelting transition occur within A-tract regions. Analyses of the energetics of the premelting transition indicate that ApA steps make a larger enthalpic contribution to the premelting transition than ApT steps. To explore the effect of cations on the premelting transition, fluorescence melts were performed in the presence of NH_4^+, Mg^{2+}, and low (0.05 M) and high (0.5 M) concentrations of Na^+. These studies show that the fluorescence intensity changes associated with the premelting transition are sensitive to cation type and concentration and are larger and more pronounced in the presence of 0.5 M Na^+, NH_4^+, and Mg^{2+}. Incorporation of 6MAP into longer duplexes containing phased A-tracts shows that the local environment of adenosines in phased A-tracts is similar to that of individual A-tracts. Fluorescence quenching results indicate that ApA and ApT steps within A-tracts are less solvent exposed than their counterparts in control sequence isomers, possibly because of the narrowed minor groove of A-tract sequences.

The study of DNA A-tracts and their unique structural properties began more than 20 years with the initial investigations of kinetoplast DNA from *Leishmania tarentolae*, which was observed to migrate anomalously on a gel relative to linear DNA (*1*). Extensive structural and biochemical studies have demonstrated that DNA molecules containing A-tracts exhibit helix bending relative to standard B-form DNA (reviewed in refs *2*−*4*). Gel migration studies have revealed that runs of four to six adenine residues in phase with the DNA helix lead to the maximum amount of curvature (*2*). In addition, structural studies of A-tract sequences containing an ApT step, such as A_3T_3, are observed to be structurally similar to A-tract sequences containing all adenines (*5*−*7*). The structural origins of A-tract-induced curvature remain a source of debate, although there is general agreement regarding the extent of global curvature of A-tract-containing sequences. The most recent solution structural studies and one crystallographic study indicate that a large portion of the sequence-induced curvature arises from non-A-tract regions at the 3′ end of the A-tract with a small contribution from the A-tract regions themselves (*8*−*10*), while other X-ray crystallographic and molecular dynamic simulations generally suggest that the sequence-induced curvature arises predominately from non-A-tract regions and that A-tract regions are relatively straight (*3*, *11*).

Runs of adenine residues have been observed in promoter regions and at the origin of replication, suggesting that DNA curvature may play an important role in these biological processes, as well as in nucleosome packaging (*12*, *13*). Significantly, the distribution of A-tracts in bacterial genomes indicates that they are over-represented, often in phase, and that they occur in clusters, which is consistent with a functional role for these sequences (*14*). Since DNA bending is an important component of many protein−DNA and drug−DNA interactions, understanding the effects of DNA

† This work was supported by a National Science Foundation Career Development Award (MCB-9507241) and a grant from the Patrick and Catherine Weldon Donaghue Medical Research Foundation. K.W. gratefully acknowledges support from an NIH training grant in Molecular Biophysics (GM08271). This research was supported in part by the Intramural Research Program of the National Institutes of Health, National Heart, Lung, and Blood Institute.

* To whom correspondence should be addressed. Phone: (860) 685-2422. Fax: (860) 685-2141. E-mail: imukerji@wesleyan.edu.

‡ Wesleyan University.

§ Present address: Optical Spectroscopy Section, Laboratory of Biophysical Chemistry, National Heart, Lung, and Blood Institute, National Institutes of Health, Building 10, Room 5D-14, Bethesda, MD 20892-1412.

|| National Cancer Institute, National Institutes of Health.

⊥ National Heart, Lung, and Blood Institute, National Institutes of Health.

10.1021/bi0518343 CCC: $33.50
Published on Web 03/25/2006

sequence on structure in those interactions is fundamental to understanding the role of DNA structure in recognition.

Structural studies of DNA A-tracts have revealed some general properties, including a progressive narrowing of the minor groove from the 5′ to 3′ end of the A-tract, significant propeller twisting of the adenine residues, formation of three-centered H-bonds, and preferential binding of ions to the minor groove (*5*, *6*, *8*, *9*, *15*−*17*). Gel migration experiments have demonstrated that the polarity of the A-tracts is important in determining their structure such that A_nT_n tracts in the 5′ to 3′ orientation migrate anomalously on a gel while a T_nA_n tract does not (*9*, *18*, *19*). Fluorescence resonance energy transfer (*20*) and NMR solution structural studies (*9*) have further confirmed that A_4T_4-containing sequences are intrinsically curved, while T_4A_4-containing sequences are not. Sequences containing A_nT_n tracts exhibit the same structural properties as A-tracts, and the most recent structural data suggest that an A_nT_n tract can be considered as two juxtaposed A-tracts (*7*, *9*). Many of the observed energetic and structural differences between A_nT_n and T_nA_n tracts have been ascribed to the structural differences between ApT and TpA steps (*9*, *21*).

A-tract-containing sequences exhibit an unusual temperature dependence, which is characterized by a premelting transition centered between 30 and 35 °C (*22*−*25*). This transition, termed the B′ to B transition, results in A-tract DNA adopting a duplex structure most similar to that of B-DNA. Although some of the molecular details of the premelting transition have been identified, such as the loss of three-centered H-bonding and propeller twisting (*26*, *27*), residue specific information has been lacking. In this study, a fluorescent adenine analogue, 4-amino-8-(2-deoxy-β-D-ribofuranosyl)-5′-*O*-dimethoxytrityl-6-methyl-7(8*H*)-pteridone (6MAP),[1] is used to probe the local environment of A-tract regions. Previously, selective replacement of adenine residues in DNA helices with fluorescent nucleoside analogues has proven to be a useful technique for gaining structural and dynamic information about DNA helices (*28*−*30*). Since 6MAP provides the same Watson−Crick H-bonding partners as adenine (Figure 1), it effectively probes the helix with minimal perturbations (*31*). In this study, the fluorescence intensity of 6MAP, which is very sensitive to base stacking interactions, is used to monitor base−base interactions during the premelting transition. Residue specific measurements are used to examine phased A-tracts and the structural differences between ApT and TpA base steps. In addition, the energetic effect of cation binding on the premelting transition as a function of cation type and charge is also examined.

MATERIALS AND METHODS

DNA Oligomers. Fluorescent oligonucleotides were prepared as previously described (*31*). Complementary strands were purchased from Integrated DNA Technologies (IDT) and were purified using a denaturing 7 M urea−20% polyacrylamide gel as described previously (*32*). Samples were brought up in a 10 mM Tris buffer (pH 7.4) containing either 0.05 M Na^+, 0.5 M Na^+, 0.05 M NH_4^+, or 0.3 M Na^+ with 0.05 M Mg^{2+}. Samples were filtered using a sterilized Whatman anatop-10 0.2 μm inorganic membrane filter. The sample concentration was determined by UV absorption spectroscopy. Duplexes were prepared by adding equal moles of the probe strand to a complementary strand. The samples were heated in a water bath at 90 °C for 5 min and then allowed to cool slowly to room temperature in the bath. All samples were stored at −20 °C. Sequences of the following fluorescent oligonucleotides were used: A3-5, 5′-CGCAFATTTCGC-3′; A3-6, 5′-CGCAAFTTTCGC; T3-8, 5′-CGCTTTAFACGC-3′; T3-7, 5′-CGCTTTFAACGC; AT-6, 5′-CGCATFTATCGC-3′; A4-8, 5′-GCGCGAAFATTTTC-

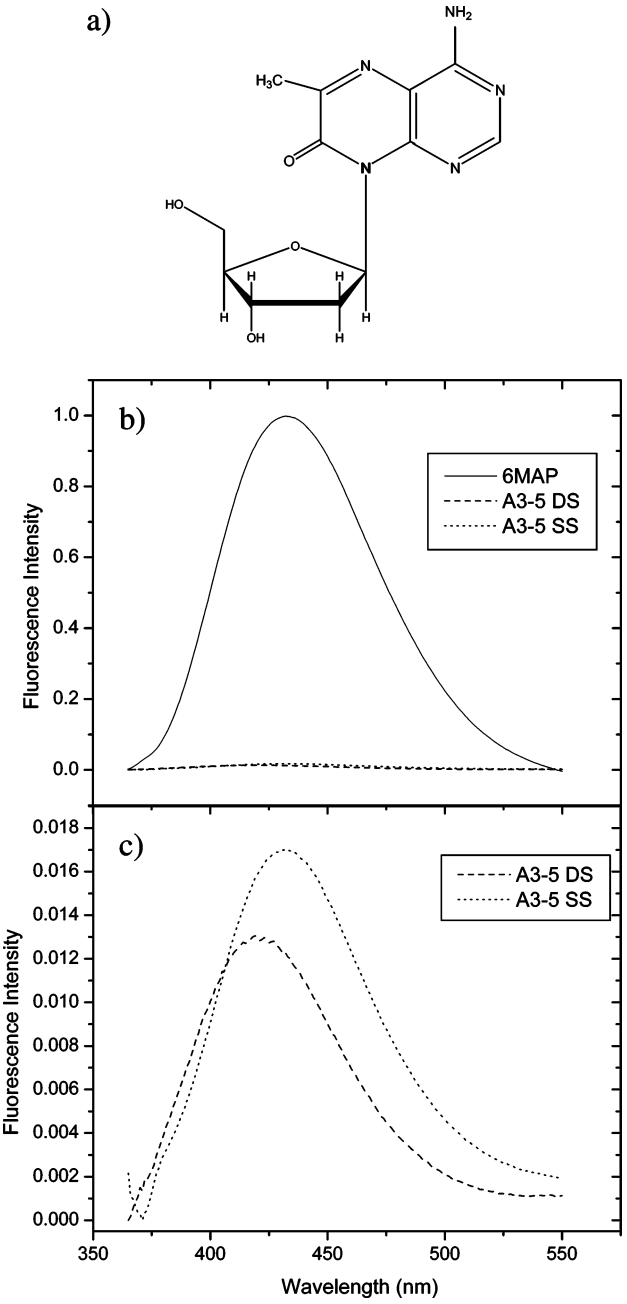

FIGURE 1: (a) Chemical structure of 6MAP. (b) Fluorescence emission spectra of the 6MAP monomer (—), single-stranded A3-5 (•••), and the A3-5 duplex (- - -) with an excitation wavelength of 330 nm. (c) Expanded view of the single-stranded A3-5 and duplex A3-5 spectra, in which the shift in peak emission wavelength upon duplex formation is readily observed. Samples were in a 10 mM Tris buffer (pH 7.4) containing 0.5 M NaCl.

[1] Abbreviations: 6MAP, 4-amino-8-(2-deoxy-β-D-ribofuranosyl)-5′-*O*-dimethoxytrityl-6-methyl-7(8*H*)-pteridone; 2-AP, 2-aminopurine; UV, ultraviolet; T_m, melting temperature; K_{SV}, Stern−Volmer quenching constant.

GAAAATTTTCCGCG-3′; A4-9, 5′-GCGCGAAAFTTTTC-GAAAATTTTCCGCG-3′; A4-19, 5′-GCGCGAAAATTTTC-GAAAFTTTTCCGCG-3′; T4-12, 5′-GCGCGTTTTAAFA-CGTTTTAAAACCGCG-3′; T4-13, 5′-GCGCGTTTTAAA-FCGTTTTAAAACCGCG-3′; and AT-12, 5′-GCGCGATATAT-FTCGATATATATCCGCG-3′.

UV Absorption Spectroscopy. DNA concentrations were determined by UV absorption spectroscopy using a Beckman-DU spectrophotometer. Single-strand samples were heated to 90 °C for 5 min before the concentrations were determined to ensure the absence of secondary structure. Absorption at 260 and 280 nm was monitored from 5 to 95 °C at a resolution of 1 °C per point and a ramp rate of 0.5 °C/min. Samples were saturated with helium before being melted, and the sample chamber was flushed with nitrogen gas to prevent condensation on the cells. T_m and van't Hoff analyses were performed using Meltwin version 3.0b (MeltCurve Processing Program courtesy of J. A. McDowell). The quality of the fits was judged by χ^2 values, which were less than 1×10^{-6}.

Fluorescence Spectroscopy. Fluorescence scans were obtained using a Jobin Yvon (Edison, NJ) SPEX Fluoromax-2 spectrofluorometer equipped with a temperature bath and a four-position sample chamber. Samples were analyzed in a cylindrical quartz cuvette and stirred continuously. Emission scans were measured from 350 to 450 nm, using slits of 5 nm band-pass and an excitation wavelength of 330 nm. Quantum yields were measured relative to 6MAP monomer and were calculated using the following equation:

$$Q_x = Q_r \frac{A_r(\lambda_r)}{A_x(\lambda_x)} \frac{I(\lambda_r)}{I(\lambda_x)} \frac{{n_x}^2}{n_r} \frac{D_x}{D_r}$$

where A is the absorbance of the sample at the excitation wavelength, I is the intensity of the exciting light at the excitation wavelength, n is the index of refraction of the solution, and D is the integrated fluorescence emission. In this case, x refers to the duplex molecules and r is the reference or 6MAP monomer.

Dodecamer duplexes were analyzed at three different salt concentrations: 0.05 M NaCl, 0.5 M NaCl, and 0.05 M NH_4Cl. The 28-mer duplexes were analyzed in either 0.3 M NaCl with 50 mM $MgCl_2$, 0.05 M NaCl, or 0.5 M NaCl. Temperature scans were performed by taking an emission scan every 5 °C from 5 to 80 °C for dodecamers and from 5 to 95 °C for the 28-mers. Temperature was controlled with a circulating water bath (RTE model 111, NESLAB Instruments, Inc.), and temperatures are accurate within ±0.1 °C. Samples were equilibrated for 2 min at the desired temperature before the spectra were acquired. Dried air was blown in the sample chamber to prevent condensation. All spectra were analyzed using Galactic GRAMS 5.2 (ThermoGalactic). A buffer spectrum was subtracted from all spectra shown. Thermodynamic parameters were calculated from the fluorescence melts using the formalism developed by Marky and Breslauer (*33*). In these analyses, the premelting transition was assumed to be a unimolecular transition and duplex and premelting transitions were analyzed independently. In the case of the B′ to B transition, the fraction of molecules in the B′ state or α was determined by the expression $\alpha(T) = [F_B(T) - F(T)]/[F_B(T) - F_{B'}(T)]$, where $F_{B'}$ corresponds to the baseline of the premelted state and F_B corresponds to the baseline of B-DNA. For the duplex transition, α corresponds to the fraction of single strands in the duplex state or $\alpha(T) = [F_{SS}(T) - F(T)]/[F_{SS}(T) - F_{DS}(T)]$, where F_{SS} is the single-stranded baseline and F_{DS} is the double-stranded baseline. Baselines were generated from linear fits to data points on either side of the transition.

This method has been shown to be sufficient for thermodynamic analysis of fluorescence data for most molecules (*34*). Fluorescence T_ms were calculated from plots of α versus temperature based on a sigmoidal fit using Microcal Origin version 6.0. The T_ms obtained by this method were in good agreement with those obtained from the maximum of the derivative plots [$d\alpha/d(1/T)$].

Time-Resolved Fluorescence Quenching. Samples were prepared with KI concentrations of 0, 0.05, 0.08, 0.15, and 0.2 M. In all solutions, a constant ionic strength of 0.2 M was maintained by addition of KCl. To prevent oxidation, 5 mM $Na_2S_2O_4$ was added to samples containing KI. Experiments were performed using a 4 MHz argon ion-pumped dye laser system and a time-correlated reverse single photon counting fluorescence apparatus as previously described (*35*). A steady-state fluorescence spectrum was obtained before and after samples were exposed to the laser to ensure that there was little to no sample degradation. Lifetime data were analyzed as a sum of exponentials, $I(\tau,\lambda) = \sum_{i=1}^{n} \alpha_i e^{-t/\tau_i}$, where I is the intensity, α_i is the pre-exponential factor or amplitude, τ_i is the lifetime, and n is the number of components (*36*). Quenching data were analyzed in terms of the Stern−Volmer equation, where K_{SV} values were determined from the longest lifetime component, such that $\tau/\tau_o = 1 + K_{SV}[Q]$, where τ is the lifetime in the presence of quencher, τ_o is the lifetime in the absence of quencher, and [Q] is the quencher concentration.

RESULTS AND DISCUSSION

Effect of Incorporation of 6MAP into Oligonucleotides. The effect of incorporation of 6MAP into the oligonucleotides selected for study was examined using UV absorption and fluorescence spectroscopic thermal melts. The relative stability of 6MAP-containing duplexes was found to be lower than that of control duplexes, despite the ability of 6MAP to base pair and form Watson−Crick hydrogen bonds with thymine residues (Figure 1). The relative thermal stability of the 6MAP-containing duplexes was compared to that of duplexes containing adenine residues by monitoring the DNA absorbance at 260 nm (Figure 2). These melting profiles revealed that incorporation of the 6MAP fluorophore into the sequence leads to an average decrease in melting temperature (T_m) of 3.2 ± 2.2 °C (Table 1 of the Supporting Information). Incorporation of 6MAP into a DNA duplex is less destabilizing than that of 2-aminopurine (2-AP), another fluorescent adenosine analogue, which was previously observed to depress the T_m of decamer duplexes approximately 10 °C compared to those of duplexes containing adenine (*28*).

Thermodynamic analysis of DNA UV melting curves resolves the energetics into enthalpic and entropic contributions (*37*, *38*), which can be compared for 6MAP-containing duplexes and control duplexes. These analyses yield $\Delta\Delta H$ values for 6MAP-containing duplexes, which exhibit a linear correlation with base stacking energies previously determined

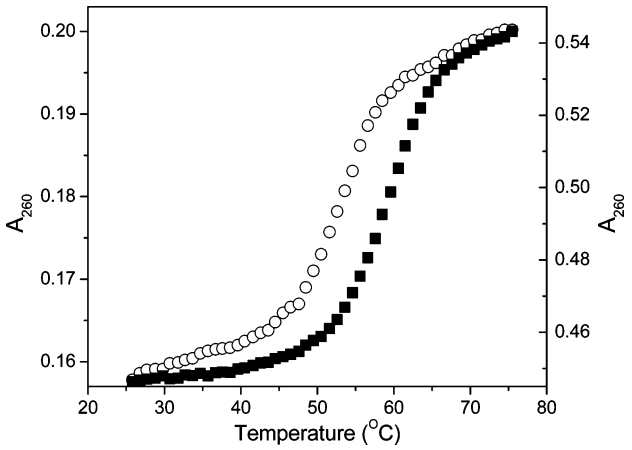

FIGURE 2: UV absorption at 260 nm of the A3-5 duplex (○, left axis) and control A3-5 duplex (■, right axis) as a function of temperature. Incorporation of 6MAP into the A3-5 duplex leads to a 6 °C depression in T_m (Table 1 of the Supporting Information). Sample conditions were as described in the legend of Figure 1.

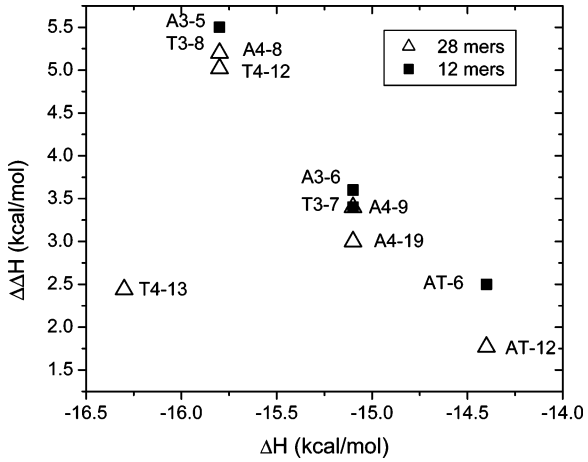

FIGURE 3: Perturbations in enthalpy arising from incorporation of 6MAP into a duplex as a function of base stacking energy. The data for 28 bp duplexes are shown as empty triangles and those for the 12 bp duplexes as filled squares. The $\Delta\Delta H$ values and local sequence environments are given in Table 1 of the Supporting Information.

by SantaLucia and co-workers (*39*) (Figure 3). The largest perturbations in ΔH are observed when 6MAP is placed in regions which make relatively large contributions to duplex stability. Thus, the largest perturbations ($\Delta\Delta H = 5.5$ kcal/mol) are observed when 6MAP is positioned between two adenine residues. This sequence (AAA) is expected to contribute −15.8 kcal/mol to the total ΔH of the duplex. Since the same $\Delta\Delta H$ values are observed for the T3-8 and A3-5 sequences, the relative polarity of the sequence does not appear to affect the degree of perturbation. Only one sequence (T4-13) has the fluorophore placed adjacent to a C·G base pair, and the energetics of this duplex are not consistent with the linear relationship determined for the other duplexes (Figure 3). This suggests that the observed linear correlation may exist only in the context of one type of nearest neighbor, and a different linear correlation may need to be developed for other sequence contexts.

Fluorescence Behavior of 6MAP. The fluorescence of 6MAP, which is strong in the monomer form (*40*), decreases approximately 90% upon incorporation into the 12 and 28-mer single strands used in this study (Figure 1b). Generation of the DNA duplexes led to a further 2−3-fold reduction in the fluorescence quantum yield, and the quantum yields of 6MAP in these single strands and duplexes exhibited some sequence dependence (Table 1 of the Supporting Information). Previous observations found that proximity to purines relative to pyrimidines caused a greater reduction in quantum yield for the pteridine nucleotide analogues (*35*, *40*). This effect is not as pronounced for 6MAP where other factors such as local sequence and structure appear to play a greater role in determining fluorescence intensity. The pronounced reduction in fluorescence intensity upon incorporation into DNA single strands or double strands is indicative that 6MAP fluorescence intensity can sensitively report on changes in stacking interactions, as previously observed for other pteridine nucleotide analogues (*32*).

Effect of Temperature on 6MAP Fluorescence. The fluorescence intensity of 6MAP and the single-stranded oligonucleotides decreases relatively linearly as a function of temperature (Figure 1 of the Supporting Information). This decrease in intensity is attributed to an increase in the relative efficiency of other relaxation processes such as internal conversion and collisional quenching, as previously observed with 2-AP (*28*).

The premelting transition in the A-tract-containing duplexes was studied by monitoring the fluorescence intensity of the duplexes as a function of temperature (Figure 4). Melting of the control dodecamer duplexes, T3-8 and AT-6, leads to an initial decrease in fluorescence intensity followed by an intensity increase as shown in Figure 4. This increase in fluorescence intensity occurs because the fluorescence yield of the single-stranded oligonucleotides is greater than that of the duplexes (Figure 1). For the AT-6 duplex, the fluorescence intensity change is the largest upon formation of the single strands relative to the other sequence isomers. This intensity change largely results from the placement of the probe between two pyrimidine residues, which leads to less quenching in the single strand relative to that with placement of the probe between two purine residues.

In addition to the duplex transition, a premelting transition, also characterized by an increase in fluorescence intensity, can be observed in the melting profile of the A3-6 duplex (Figure 4). This transition is not observed in the sequence isomers containing T_3A_3 or $(AT)_3$ sequences. Similarly, a premelting transition is only observed in the 28 bp duplexes that contain an A-tract (Figure 4b) compared to the T_4A_4- and $(AT)_4$-containing duplexes. The potential influence of 6MAP on the melting behavior cannot be discounted; however, this influence should also be manifested in the control duplexes, which show no evidence of a premelting transition (Figure 4).

The concomitant increase in fluorescence intensity is consistent with a decrease in the level of stacking interactions accompanying the B′ to B transition. Since each duplex contains only one 6MAP monomer, the fluorescence arises from only one site in the duplex and the intensity changes likely reflect conformational changes proximate to 6MAP. The site specificity of the fluorescence also causes it to be more sensitive to the B′ to B transition than in UV absorbance measurements which exhibit less pronounced transitions (compare Figures 2 and 4). This site specific fluorescence measurement is also indicative that some of the

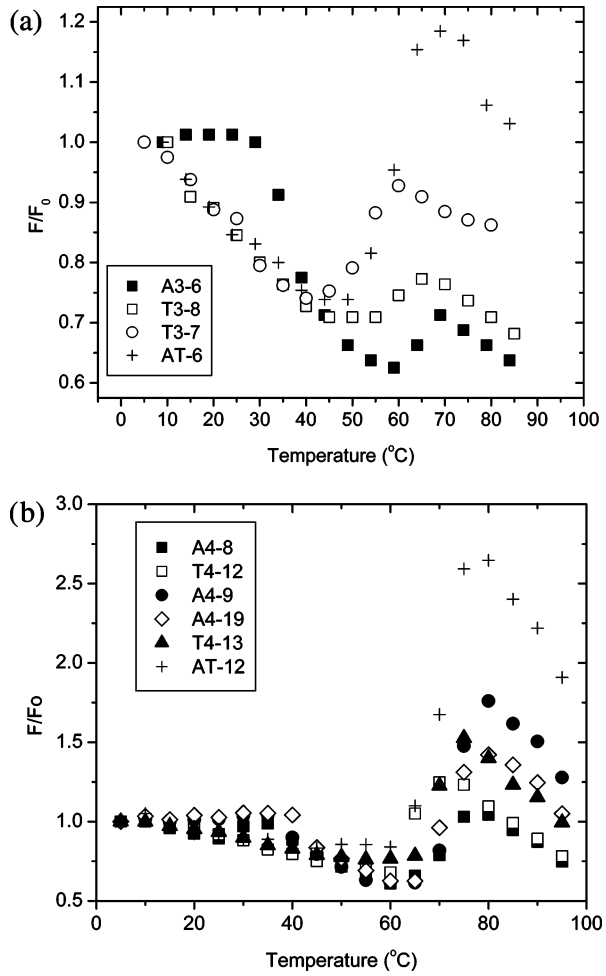

FIGURE 4: (a) Fluorescence intensity of the A3-6 (■), AT-6 (+), T3-8 (□), and T3-7 (○) duplexes as a function of temperature. All fluorescence intensities shown are relative to the initial fluorescence intensity (F_o). Measurements were performed in a 0.5 M NaCl, 10 mM Tris buffer at pH 7.4. (b) Fluorescence intensity of the A4-8 (■), A4-9 (●), A4-19 (◇) T4-12 (□), T4-13 (▲), and AT-12 (+) duplexes as a function of temperature. All fluorescence intensities shown are relative to the fluorescence intensity at 5 °C (F_o). Measurements were performed in 0.3 M NaCl with 0.05 M Mg^{2+} in a 10 mM Tris buffer at pH 7.4.

conformational changes associated with the B′ to B transition occur in A-tract regions. This can come from changes in local stacking interactions or helix unwinding.

Energetics of the Premelting Transition. The enthalpic and entropic components of the premelting transition were determined by a van't Hoff analysis following the formalism of Marky and Breslauer (*33*) (Table 1). In these analyses, linear baselines were extrapolated from data points on either side of the transition and the fraction of single strands in the B′ form, α, was monitored as a function of temperature. Thus, α is expected to decrease from a value of 1 with an increase in temperature. These analyses yielded sigmoidal curves for the premelting transition, consistent with the previously observed cooperativity of A-tract behavior (*19*) (Figure 5).

Since 6MAP was incorporated into specific sites, residue specific information can be gained regarding the premelting transition. In the 12 and 28 bp A-tract duplexes, the 6MAP probe was incorporated at either an ApA or an ApT base step. The melting profiles that were obtained (Figure 5) indicate that when the 6MAP is incorporated at an ApT step a lower melting temperature and less cooperativity are observed (compared to those for incorporation of 6MAP at an ApA step). In the case of the 12 bp duplexes, the analysis reveals a difference of approximately 13 °C between ApA and ApT base steps, while a difference of only 7 °C is observed for the 28 bp duplexes (Table 1). These differences in melting behavior and T_m are also reflected in the determination of the $\Delta H_{premelt}$. For both the 12 and 28 bp duplexes, the $\Delta H_{premelt}$ of the ApA step is 1.5−2 times larger than the $\Delta H_{premelt}$ observed for the ApT step (Table 1). In addition, the values of $\Delta H_{premelt}$ measured relative to the total number of A·T base pairs are lower for the 28 bp duplexes than for the 12 bp duplexes. This difference could be a consequence of the increased length of the A-tract regions.

Although the incorporation of the 6MAP probe necessarily perturbs the structure, we note that the ApT and ApA steps yield duplex melting curves which are consistent with those obtained by UV absorption (Figure 2 of the Supporting Information). Comparisons of UV absorption duplex melting curves of control and 6MAP-containing duplexes indicate that the ApA step is most perturbed by the incorporation of 6MAP. Since the premelt is not readily observed in the UV absorption data, these comparisons cannot be made for the premelting transition. If the effect of incorporation of 6MAP on the premelting transition is the same as that for the duplex transition, then $\Delta H_{premelt}$ for ApA steps should be lower than that for the ApT steps. Since the current findings suggest that ApA steps are more stable than ApT steps (with respect to the premelting transition), the differences in stability do not appear to arise from 6MAP incorporation but rather appear to arise from the A-tracts themselves. These findings are consistent with previous NMR studies, which measured base pair opening kinetics for A-tract sequences and determined that the last A·T base pair of the tract has the shortest lifetime relative to those of the A·T base pairs in the central region of the tract (*41*).

The increased stability of ApA steps relative to ApT steps with respect to the premelting transition is similar to the behavior observed with respect to duplex melting, although the effects in the premelting transition are more pronounced. The greater stability observed for ApA steps probably arises in part from the greater enthalpic contribution of the AA/TT base pair stack relative to the AT/TA base pair stack (*38*, *39*).

In A_4T_4-containing sequences, it has been observed that the minor groove is the narrowest at the central ApT step and this step has a high negative roll, leading to a local bend toward the minor groove (*9*). In addition, it has been previously observed by both X-ray crystallography and NMR spectroscopy that adenosine residues in A-tract regions exhibit a large degree of propeller twisting (−15°) (*2*). The increase in fluorescence intensity observed for the premelting transition is attributed to a reduction in the level of base stacking interactions, which could potentially be caused by a change in either one or both of these helicoidal parameters, since both would perturb the base stacking interactions critical to yield. These findings are consistent with previous UV resonance Raman studies in which a decrease in the level of base stacking interactions and hypochromism was observed during the premelting transition for similar A-tract-containing dodecamer duplexes (*27*).

Table 1: Thermodynamics of the Premelting Transition As Measured with 6MAP

duplex	local environment[a]	[M^+] (M)	T_m (°C)	$\Delta H_{premelt}$ (kcal/mol)[b]	ΔH (kcal/mol of A·T base pairs)[b]	% $\Delta H_{premelt}$[c]
A3-5	AFA	0.5 Na^+	30 ± 2	64.3 ± 6.4	10.7	0.38
A3-5	AFA	0.05 NH_4^+	22 ± 2	50.2 ± 5.0	8.4	0.40
A4-8	AFA	0.5 Na^+	31 ± 2	66.9 ± 6.7	4.2	NA[d]
A4-8	AFA	0.3 Na^+ and 0.05 Mg^{2+}	30 ± 2	68.9 ± 6.9	4.3	0.41
A3-6	AFT	0.5 Na^+	17 ± 2	34.3 ± 3.4	5.7	0.30
A3-6	AFT	0.05 NH_4^+	12 ± 2	35.1 ± 3.5	5.8	0.30
A4-9	AFT	0.5 Na^+	27 ± 2	27.2 ± 2.7	1.7	NA[d]
A4-9	AFT	0.3 Na^+ and 0.05 Mg^{2+}	19 ± 2	24.1 ± 2.4	1.5	0.17
A4-19	AFT	0.5 Na^+	26 ± 2	22.0 ± 2.2	1.4	NA[d]
A4-19	AFT	0.3 Na^+ and 0.05 Mg^{2+}	20 ± 2	20.6 ± 2.1	1.3	0.17

[a] Sequences are reported in the 5′ to 3′ direction. [b] Determined from a van't Hoff analysis of the premelting transition as measured by fluorescence. [c] $\Delta H_{premelt}/\Delta H_{total} \times 100$; ΔH_{total} determined from independent van't Hoff analyses of both the premelting and duplex transitions as measured by fluorescence. [d] The duplex transition is not fully observed under these conditions.

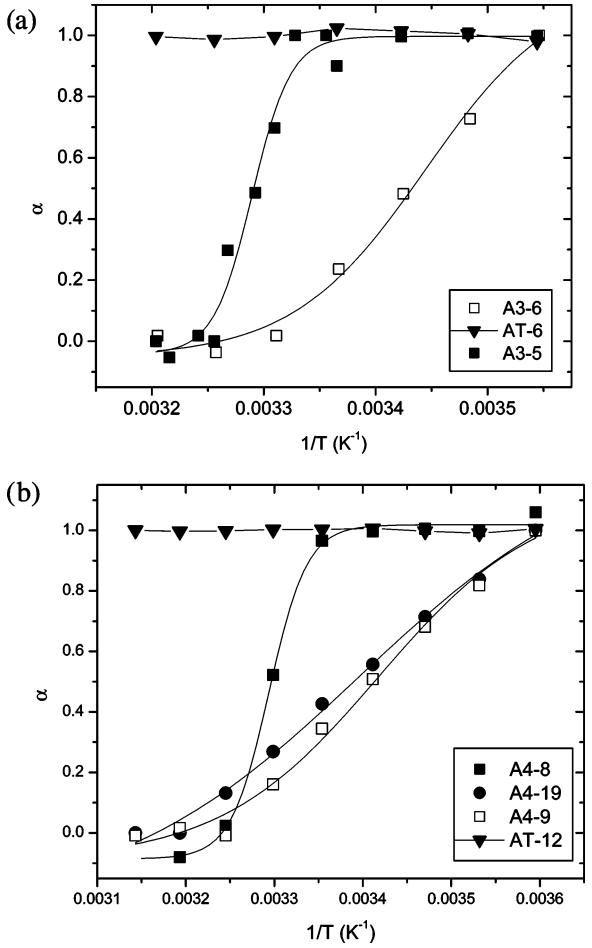

FIGURE 5: (a) Fraction of molecules in the premelted or B′ state (α) as a function of temperature for the A3-5 (■), A3-6 (□), and AT-6 (▼) duplexes. Sigmoidal fits to the A3-5 and A3-6 data are shown as solid lines. The T_m(B′) of the A3-6 duplex is 13 °C lower than that of the A3-5 duplex. (b) Fraction of molecules in the premelted or B′ state (α) as a function of temperature for the A4-8 (■), A4-9 (□), A4-19 (●), and AT-12 (▼) duplexes. Sigmoidal fits to the A4-8, A4-9, and A4-19 data are shown as solid lines. The T_m(B′) values of the A4-9 and A4-19 duplexes are 10−11 °C lower than that of the A4-8 duplex. For the control duplexes, AT-6 and AT-12, the fraction of molecules in the initial state remains constant at 1.0 over the temperature range that is depicted.

Effect of Phased A-Tracts on the Premelting Transition. The premelting transition was also examined in the context of two phased A-tract sequences. Melting profiles of 6MAP residues in either the first or second A-tract (A4-9 or A4-19, respectively) are quite similar and suggest that the local environment within each A-tract is approximately the same (Figure 5b). In both duplexes, 6MAP is located at an ApT step and the $\Delta H_{premelt}$ values, determined from fluorescence melting curves of the A4-9 and A4-19 duplexes, are within 4−5 kcal of each other (27 and 22 kcal/mol, respectively, in 0.5 M Na^+) (Table 1). This value is relatively small when compared to the 40 kcal/mol difference in $\Delta H_{premelt}$ between ApA and ApT base steps. The premelting transition occurs at a lower temperature than in the A4-8 duplex (Table 1), in which the 6MAP is incorporated at an ApA step and the similarity of the phased environments is consistent with the cooperativity of A-tract behavior (*19*).

Solvent Accessibility of ApT versus TpA. The relative solvent accessibility of the 6MAP probe within the dodecamer duplexes was examined using time-resolved fluorescence spectroscopy. For all of the dodecamer duplexes that have been studied, the lifetimes are close in value to those observed for 6MAP in the single strand. The absence of a large change in lifetime upon formation of the duplex is suggestive that the primary mechanism of quenching for 6MAP upon formation of the duplex is one of static quenching, as reported previously (*40*).

The simplest description of the data yields two lifetimes for all the dodecamer duplexes: (1) a longer lifetime component of 4.5−5.1 ns, which is comparable to that of the free monomer, and (2) a shorter component of 0.1−0.6 ns (Figure 3 of the Supporting Information). The majority of the observed fluorescence intensity arises from the long-lived component, which is attributed to the probe adopting a conformation with greater solvent exposure, as has been previously observed with 2-AP (*28*). Consistent with this assignment, we find that the lifetime of this component is most strongly affected by KI quenching and that the determined quenching constants (K_{SV} values) are within 56−83% of a diffusion-controlled reaction (Figure 6) (*42*). The shorter lifetime component is attributed to conformations in which the probe is stacked within the helix and experiences collisional contacts with the sugar backbone or other bases. In the decay-associated spectra (Figure 4 of the Supporting Information), this component peaks at shorter wavelengths relative to the long-lived component, in agreement with the −9 nm shift in peak emission of the duplexes relative to free monomer.

Stern−Volmer analysis of the longest-lived component as a function of KI concentration (*43*) reveals that the probe is

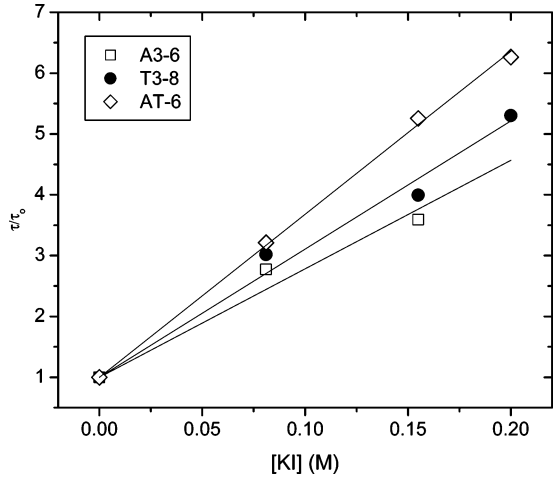

FIGURE 6: Stern−Volmer plot of the longest lifetime components of the A3-6 (□), T3-8 (●), and AT-6 duplexes (◇). Measurements were performed in 0.0, 0.08, 0.15, and 0.20 M KI solutions with 5 mM $Na_2S_2O_4$ in a 10 mM Tris buffer at pH 7.4. KCl was added to maintain a constant ionic strength of 0.2 M. K_{SV} values are given in Table 2.

Table 2: Solvent Accessibility Determined from Time-Resolved Fluorescence Experiments and KI Quenching

sequence name	local environment[a]	K_{SV} (M^{-1})[b]
A3-5	AFATTT	19.7 ± 1.5
A3-6	AAFTTT	17.8 ± 1.5
T3-8	TTTAFA	21.1 ± 0.9
T3-7	TTTFAA	20.4 ± 0.6
AT-6	ATFTAT	26.6 ± 0.3

[a] Sequences are reported in the 5′ to 3′ direction. [b] K_{SV} values determined from the longest lifetime component as described in Materials and Methods.

most solvent exposed when placed between two thymine residues as in the AT-6 duplex (K_{SV} = 26.6 M^{-1}) (Figure 6). The least solvent accessible position is associated with the A3-6 duplex (K_{SV} = 17.8 M^{-1}), in which the probe is situated between adenine and thymine residues at the 3′ end of the A-tract. Although K_{SV} values for the sequence isomers fall within a relatively narrow range, the values for adenine residues within the A-tracts are consistently lower than their counterparts in the T3-8, T3-7, and AT-6 duplexes (Table 2). This reduced solvent accessibility is attributed to the narrow minor groove and better base stacking observed in A-tract regions (*2*). An understanding of the difference in solvent accessibility between ApT and TpA base steps can be gained from structural studies of A-tract sequences. The minor groove was observed to be the narrowest at the ApT step in an A_4T_4-containing sequence by NMR, while in T_4A_4-containing sequences, the 3′ to 5′ orientation of the A-tracts leads to a widening of the minor groove at the TpA step (*5*, *9*). We suggest that the decreased solvent accessibility of the ApT step is consistent with the progressive 5′−3′ narrowing of the A-tract minor groove as observed by NMR (*9*), hydroxyl radical footprinting (*44*), and uranyl photocleavage experiments (*7*).

Effect of Cations on the B′ to B Transition. Observation of the premelting transition by 6MAP fluorescence appears to be dependent on both cation type and concentration. For the dodecamer duplexes, 0.05 M Na^+ is not sufficient for observing the premelting transition (Figure 7a), while a premelting transition is observed in the presence of a 10-

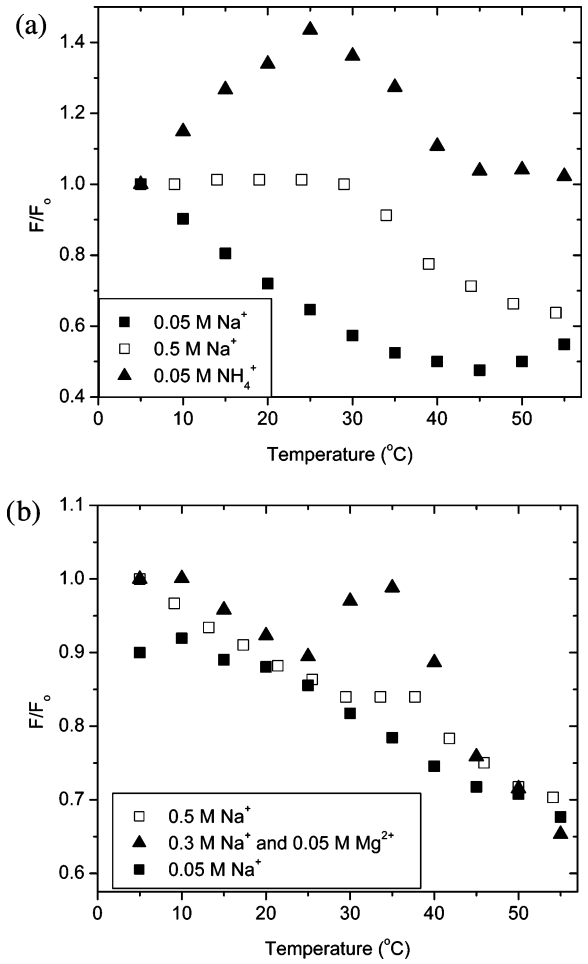

FIGURE 7: Effect of cations on the premelting transition. (a) Fluorescence intensity of the A3-6 duplex as a function of temperature in the presence of 0.05 M Na^+ (■), 0.5 M Na^+ (□), or 0.05 M NH_4^+ (▲). (b) Fluorescence intensity of the A4-8 duplex as a function of temperature in the presence of 0.05 M Na^+ (■), 0.5 M Na^+ (□), or 0.3 M Na^+ and 0.05 M Mg^{2+} (▲). The 0.05 M Na^+ data are shown with an offset of −0.1 for clarity. All fluorescence intensities that are shown are relative to the fluorescence intensity at 5 °C (F_o).

fold increase in Na^+ concentration to 0.5 M. In contrast to Na^+, a premelting transition is detected in the presence of 0.05 M NH_4^+, and the magnitude of the fluorescence change is larger in the presence of NH_4^+ than in the presence of 0.5 M Na^+ (Figure 7a). In the presence of 0.05 M NH_4^+, the premelting transition occurs at a lower temperature relative to that observed in 0.5 M Na^+ [30 °C vs 22 °C for the ApA step (Table 1)]. This difference can be attributed in part to the 10-fold difference in cation concentration. Interestingly, the magnitude of the premelting transition relative to the duplex transition is approximately the same regardless of cation type [38% for the ApA step and 29% for the ApT step (Table 1)]. This observation suggests that the two transitions exhibit a similar dependence on cation type and concentration in this instance.

In the case of the 28 bp duplexes as with the 12 bp duplexes, 0.05 M Na^+ is not sufficient to induce a premelting transition, while 0.5 M Na^+ is (Figure 7b). Addition of 0.05 M Mg^{2+} in place of 0.2 M Na^+ enhances the intensity of the fluorescence change associated with the transition (Figure 7b). The T_m of the transition is slightly lower in the presence of Mg^{2+} [33 vs 30 °C for the ApA step (Table 1)], consistent

with the lower ionic strength of the solution (Figure 7b). For the ApA step, the relative magnitude of the premelting transition compared to the duplex transition is 41%, similar to the values obtained with the dodecamer duplexes. In the case of 0.5 M Na^+, relative measurements cannot be made because the duplex transition occurs above 85 °C and is not fully observed.

Since 6MAP fluorescence is strongly anticorrelated with the amount of stacking the probe experiences, the differences in the fluorescence intensity associated with the premelting transition probably result from differences in the stacking interactions of the probe as a consequence of ion binding and changes in local conformation.

Although the effect of cations on the premelting transition has not been a subject of extensive study, the effect of cation binding on the structure of DNA A-tracts has been examined by a number of different methods (*3*, *6*, *45*, *46*). In general, metal ion binding sites are observed in the narrowed minor groove of the A-tract region. The effect of Na^+ concentration on A-tract structure has been examined by FRET, and a greater degree of bending was observed at higher concentrations of Na^+ up to 0.5 M (*47*). Detection of DNA shape by NMR spectroscopy (*48*) and topological measurements of bend angle (*49*) indicate that Mg^{2+} induces a greater degree of bending than Na^+ alone. Similarly, gel mobility experiments suggest that NH_4^+ also induces a greater amount of bending than Na^+ (*9*), while NMR studies indicate that NH_4^+ can displace Na^+ in the minor groove at the ApT step (*6*). In this work, the premelting transition is cation-dependent and the largest fluorescence intensity changes in the premelting transition are observed in the presence of NH_4^+ and Mg^{2+} (Figure 7). Since binding of these two ions has also been shown to lead to a greater amount of DNA bending, it appears that the relative fluorescence intensity change associated with the premelting transition can be correlated with DNA bending. The increased intensity of the premelting transition in the presence of Mg^{2+} and NH_4^+ is also consistent with the model of sequence-directed curvature stabilized by cation localization in the minor groove (*4*).

In these A-tract sequences, a spine of hydration is also expected to occur in the narrowed minor groove and the ion effects cannot be completely decoupled from those of hydration. In general, A-tract sequences have been found to be more hydrated than the control sequences and hydration has been shown to contribute significantly to the stability of these sequences (*50, 51*). In our study, hydration undoubtedly plays a role; however, the fluorescence experiments do not explicitly examine the effect of hydration on the premelting transition.

SUMMARY

The fluorescent adenosine analogue, 6MAP, has been used to site specifically probe the premelting transition in DNA A-tracts. We observe that 6MAP monitors the premelting transition more sensitively than UV absorbance and potentially provides a better method for monitoring this transition. Energetic analyses of A-tract-containing duplexes reveal that ApT base steps have a lower $\Delta H_{premelt}$ than ApA steps and that ApT steps undergo the premelting transition at lower temperatures. The fluorescence intensity changes associated with the premelting transition are more pronounced in the presence of NH_4^+ and Mg^{2+} than in the presence of Na^+, and lower concentrations of these ions are needed to induce the transition. The cation-dependent fluorescent behavior correlates with the amount of DNA bending as measured by other methods. This study demonstrates the utility of a 6MAP residue specific analysis approach for studying the structure and energetics of DNA A-tracts. In future work, a similar approach can be used to further explore the effect of cations on the transition and study the conformation of non-A-tract regions in A-tract-containing sequences.

ACKNOWLEDGMENT

We thank Dr. John Harvey (National Institutes of Health) for his assistance in acquiring the fluorescence lifetime data.

SUPPORTING INFORMATION AVAILABLE

One table detailing the physical characteristics of the 6MAP-containing duplexes, the fluorescence intensity of the 6MAP monomer and the A3-5 single-stranded oligonucleotide as a function of temperature (Figure 1), the duplex to single-strand transition of the A4-8, A4-9, and A4-19 duplexes (Figure 2), a representative fluorescence decay of a 6MAP-containing duplex with associated fit and residuals (Figure 3), and a decay-associated spectrum for a 6MAP-containing duplex (Figure 4). This material is available free of charge via the Internet at http://pubs.acs.org.

REFERENCES

1. Marini, J. C., Levene, S. D., Crothers, D. M., and Englund, P. T. (1982) Bent Helical Structure in Kinetoplast DNA, *Proc. Natl. Acad. Sci. U.S.A. 79*, 7664−8.
2. Crothers, D. M., and Shakked, Z. (1999) DNA Bending by adenine-thymine tracts, in *Oxford Handbook of Nucleic Acid Structure* (Neidle, S., Ed.) pp 455−70, Oxford University Press, Oxford, U.K.
3. Beveridge, D. L., Dixit, S. B., Barreiro, G., and Thayer, K. M. (2004) Molecular dynamics simulations of DNA curvature and flexibility: Helix phasing and premelting, *Biopolymers 73*, 380−403.
4. Hud, N. V., and Plavec, J. (2003) A unified model for the origin of DNA sequence-directed curvature, *Biopolymers 69*, 144−58.
5. Hud, N. V., and Feigon, J. (2002) Characterization of divalent cation localization in the minor groove of the A_nT_n and T_nA_n DNA sequence elements by ^1H NMR spectroscopy and manganese(II), *Biochemistry 41*, 9900−10.
6. Hud, N. V., Sklenar, V., and Feigon, J. (1999) Localization of ammonium ions in the minor groove of DNA duplexes in solution and the origin of DNA A-tract bending, *J. Mol. Biol. 286*, 651−60.
7. Mollegaard, N. E., Lindemose, S., and Nielsen, P. E. (2005) Uranyl photoprobing of nonbent A/T- and bent A-tracts. A difference of flexibility? *Biochemistry 44*, 7855−63.
8. MacDonald, D., Herbert, K., Zhang, X., Pologruto, T., Lu, P., and Polgruto, T. (2001) Solution structure of an A-tract DNA bend, *J. Mol. Biol. 306*, 1081−98.
9. Stefl, R., Wu, H., Ravindranathan, S., Sklenar, V., and Feigon, J. (2004) DNA A-tract bending in three dimensions: Solving the dA4T4 vs dT4A4 conundrum, *Proc. Natl. Acad. Sci. U.S.A. 101*, 1177−82.
10. Hizver, J., Rozenberg, H., Frolow, F., Rabinovich, D., and Shakked, Z. (2001) DNA bending by an adenine-thymine tract and its role in gene regulation, *Proc. Natl. Acad. Sci. U.S.A. 98*, 8490−5.
11. Yoon, C., Prive, G. G., Goodsell, D. S., and Dickerson, R. E. (1988) Structure of an alternating-B DNA helix and its relationship to A-tract DNA, *Proc. Natl. Acad. Sci. U.S.A. 85*, 6332−6.
12. Sinden, R. R. (1994) *DNA Structure and Function*, Academic Press, San Diego.
13. Koch, K. A., and Thiele, D. J. (1999) Functional Analysis of a Homopolymeric (dA-dT) Element That Provides Nucleosomal

Access to Yeast and Mammalian Transcription Factors, *J. Biol. Chem. 274*, 23752−60.
14. Tolstorukov, M. Y., Virnik, K. M., Adhya, S., and Zhurkin, V. B. (2005) A-tract clusters may facilitate DNA packaging in bacterial nucleoid, *Nucleic Acids Res. 33*, 3907−18.
15. Shatzky-Schwartz, M., Arbuckle, N. D., Eisenstein, M., Rabinovich, D., Bareket-Samish, A., Haran, T. E., Luisi, B. F., and Shakked, Z. (1997) X-ray and Solution Studies of DNA Oligomers and Implications for the Structural Basis of A-tract-dependent Curvature, *J. Mol. Biol. 267*, 595−623.
16. Edwards, K. J., Brown, D. G., Spink, N., Skelly, J. V., and Neidle, S. (1992) Molecular Structure of the B-DNA Dodecamer d(CG-CAAATTTGCG)$_2$: An Examination of Propeller Twist and Minor-groove Water Structure at 2.2 Å Resolution, *J. Mol. Biol. 226*, 1161−73.
17. Nelson, H. C. M., Finch, J. T., Luisi, B. F., and Klug, A. (1987) The Structure of an oligo(dA)·oligo(dT) Tract and its Biological Implications, *Nature 330*, 221−6.
18. Hagerman, P. J. (1986) Sequence-directed curvature of DNA, *Nature 321*, 449.
19. Haran, T. E., and Crothers, D. M. (1989) Cooperativity in A-Tract Structure and Bending Properties of Composite T_nA_n Blocks, *Biochemistry 28*, 2763−7.
20. Wojtuszewski, K., and Mukerji, I. (2003) HU Binding to Bent DNA: A Fluorescence Anisotropy and Resonance Energy Transfer Study, *Biochemistry 42*, 3096−104.
21. Crothers, D. M., Haran, T. E., and Nadeau, J. G. (1990) Intrinsically bent DNA, *J. Biol. Chem. 265*, 7093−6.
22. Park, Y.-W., and Breslauer, K. J. (1991) A Spectroscopic and Calorimetric Study of the Melting Behaviors of a 'bent' and 'normal' DNA Duplex: [d(GA$_4$T$_4$C)]$_2$ versus [d(GT$_4$A$_4$C)]$_2$, *Proc. Natl. Acad. Sci. U.S.A. 88*, 1551−5.
23. Chan, S. S., Breslauer, K. J., Hogan, M. E., Kessler, D. J., Austin, R. H., Ojemann, J., Passner, J. M., and Wiles, N. C. (1990) Physical Studies of DNA Premelting Equilibria in Duplexes with and without Homo dA*dT Tracts: Correlations with DNA Bending, *Biochemistry 29*, 6161−71.
24. Breslauer, K. J. (1991) A Thermodynamic Perspective of DNA Bending, *Curr. Opin. Struct. Biol. 1*, 416−22.
25. Chan, S. S., Breslauer, K. J., Austin, R. H., and Hogan, M. E. (1993) Thermodynamics and premelting conformational changes of phased (dA)$_5$ tracts, *Biochemistry 32*, 11776−84.
26. Chan, S. S., Austin, R. H., Mukerji, I., and Spiro, T. G. (1997) Temperature-dependent ultraviolet resonance Raman spectroscopy of the premelting state of dA·dT DNA, *Biophys. J. 72*, 1512−20.
27. Mukerji, I., and Williams, A. P. (2002) UV resonance Raman and circular dichroism studies of a DNA duplex containing an A$_3$T$_3$ tract: Evidence for a premelting transition and three-centered H-bonds, *Biochemistry 41*, 69−77.
28. Xu, D., Evans, K. O., and Nordlund, T. M. (1994) Melting and Premelting Transitions of an Oligomer Measured by DNA Base Fluorescence and Absorption, *Biochemistry 33*, 9592−9.
29. Larsen, O. F., van Stokkum, I. H., Gobets, B., van Grondelle, R., and van Amerongen, H. (2001) Probing the structure and dynamics of a DNA hairpin by ultrafast quenching and fluorescence depolarization, *Biophys. J. 81*, 1115−26.
30. Johnson, N. P., Baase, W. A., and Von Hippel, P. H. (2004) Low-energy circular dichroism of 2-aminopurine dinucleotide as a probe of local conformation of DNA and RNA, *Proc. Natl. Acad. Sci. U.S.A. 101*, 3426−31.
31. Hawkins, M. E. (2001) Fluorescent pteridine nucleoside analogs: A window on DNA interactions, *Cell. Biochem. Biophys. 34*, 257−81.
32. Wojtuszewski, K., Hawkins, M. E., Cole, J. L., and Mukerji, I. (2001) HU Binding to DNA: Evidence for Multiple Complexes and DNA Bending, *Biochemistry 40*, 2588−98.
33. Marky, L. A., and Breslauer, K. J. (1987) Calculating Thermodynamic Data for Transitions of any Molecularity from Equilibrium Melting Curves, *Biopolymers 26*, 1601−20.
34. Vamosi, G., and Clegg, R. M. (1998) The helix-coil transition of DNA duplexes and hairpins observed by multiple fluorescence parameters, *Biochemistry 37*, 14300−16.
35. Hawkins, M. E., Pfleiderer, W., Balis, F. M., Porter, D., and Knutson, J. R. (1997) Fluorescence Properties of Pteridine Nucleoside Analogs as Monomers and Incorporated into Oligonucleotides, *Anal. Biochem. 244*, 86−95.
36. Knutson, J. R., Beechem, J. M., and Brand, L. (1983) Simultaneous Analysis of Multiple Fluorescence Decay Curves: A Global Approach, *Chem. Phys. Lett. 102*, 501−7.
37. Turner, D. H. (1996) Thermodynamics of base pairing, *Curr. Opin. Struct. Biol. 6*, 299−304.
38. SantaLucia, J., Jr., Allawi, H. T., and Seneviratne, P. A. (1996) Improved nearest-neighbor parameters for predicting DNA duplex stability, *Biochemistry 35*, 3555−62.
39. Allawi, H. T., and SantaLucia, J., Jr. (1997) Thermodynamics and NMR of internal G·T mismatches in DNA, *Biochemistry 36*, 10581−94.
40. Hawkins, M. E., Pfleiderer, W., Jungmann, O., and Balis, F. M. (2001) Synthesis and Fluorescence Characterization of Pteridine Adenosine Nucleoside Analogs for DNA Incorporation, *Anal. Biochem. 298*, 231−40.
41. Leroy, J.-L., Charretier, E., Kochoyan, M., and Gueron, M. (1988) Evidence from Base-Pair Kinetics for Two Types of Adenine Tract Structures in Solution: Their Relation to DNA Curvature, *Biochemistry 27*, 8894−8.
42. Eftink, M. R., and Ghiron, C. A. (1981) Fluorescence quenching studies with proteins, *Anal. Biochem. 114*, 199−227.
43. Lakowicz, J. R. (1999) *Principles of Fluorescence Spectroscopy*, 2nd ed., Kluwer Academic/Plenum, New York.
44. Burkhoff, A. M., and Tullius, T. D. (1988) Structural Details of an Adenine Tract That Does Not Cause DNA to Bend, *Nature 331*, 455−7.
45. Shui, X., McFail-Isom, L., Hu, G. G., and Williams, L. D. (1998) The B-DNA dodecamer at high resolution reveals a spine of water on sodium, *Biochemistry 37*, 8341−55.
46. Young, M. A., Jayaram, B., and Beveridge, D. L. (1997) Intrusion of Counterions into the Spine of Hydration in the Minor Groove of B-DNA: Fractional Occupancy of Electronegative Pockets, *J. Am. Chem. Soc. 119*, 59−69.
47. Toth, K., Sauermann, V., and Langowski, J. (1998) DNA Curvature in Solution Measured by Fluroescence Resonance Energy Transfer, *Biochemistry 37*, 8173−9.
48. Jerkovic, B., and Bolton, P. H. (2001) Magnesium increases the curvature of duplex DNA that contains dA tracts, *Biochemistry 40*, 9406−11.
49. Tchernaenko, V., Halvorson, H. R., and Lutter, L. C. (2004) Topological measurement of an A-tract bend angle: Effect of magnesium, *J. Mol. Biol. 341*, 55−63.
50. Marky, L. A., and Kupke, D. W. (1989) Probing the hydration of the minor groove of A·T synthetic DNA polymers by volume and heat changes, *Biochemistry 28*, 9982−8.
51. Marky, L. A., and Macgregor, R. B., Jr. (1990) Hydration of dA·dT polymers: Role of water in the thermodynamics of ethidium and propidium intercalation, *Biochemistry 29*, 4805−11.

BI0518343